

Journal of Materials Chemistry C

Accepted Manuscript



This is an *Accepted Manuscript*, which has been through the Royal Society of Chemistry peer review process and has been accepted for publication.

Accepted Manuscripts are published online shortly after acceptance, before technical editing, formatting and proof reading. Using this free service, authors can make their results available to the community, in citable form, before we publish the edited article. We will replace this *Accepted Manuscript* with the edited and formatted *Advance Article* as soon as it is available.

You can find more information about *Accepted Manuscripts* in the [Information for Authors](#).

Please note that technical editing may introduce minor changes to the text and/or graphics, which may alter content. The journal's standard [Terms & Conditions](#) and the [Ethical guidelines](#) still apply. In no event shall the Royal Society of Chemistry be held responsible for any errors or omissions in this *Accepted Manuscript* or any consequences arising from the use of any information it contains.

Tri-Wavelength Broadband Antireflective Coating built from refractive index controlled MgF₂ films

Cite this: DOI: 10.1039/x0xx00000x

Ruimin Ding,^a Xinmin Cui,^{ab} Cong Zhang,^{ab} Ce Zhang^{ab} and Yao Xu^{*a}

Received 00th January 2012,
Accepted 00th January 2012

DOI: 10.1039/x0xx00000x

www.rsc.org/

Regulation on the refractive index over wide range is very important in the realization of tri-wavelength antireflective (AR) coating in high power laser system, but many regulation approaches are too complex or violent to satisfy the practical requirements. Here, a simple, template-free sol-gel route was proposed to regulate the refractive index of MgF₂ film by heat treating MgF₂ sol and hence to control the self-assembly process of colloidal MgF₂ nanocrystals. In this self-assembly process, the originally packed nanocrystals gradually evolved to bigger hollow vesicles, which reduced the refractive index of the MgF₂ film from 1.38 to 1.2. When the refractive indices of the bottom and top layers were set as 1.34 and 1.2, the tri-wavelength broadband AR coating was finally realized on quartz substrate, with the transmittance of 99.54%, 98.65% and 98.58% at 351 nm, 527 nm and 1053 nm, respectively.

Introduction

Since broadband antireflective (AR) coatings became increasingly important in a wide variety of optical technology by reducing reflective losses at interfaces over a broad range of wavelengths, the regulation of refractive index (*n*), as the most fundamental requirement of an AR system, has been extensively explored.¹⁻³ Its realization relies on the principle of incorporating designed nonporous structures into the coatings, such as sol-gel processes,⁴ reactive ion etching,⁵ self-assembly of degradable block copolymer,⁶ phase separation of a binary polymer blend⁷ and layer-by-layer (LBL) assembly of hollow silica nanoparticles.⁸

In high power laser system, some optical elements must be subjected to the simultaneous transmission of light of three wavelengths (1053 nm, 527 nm and 351 nm) owing to the conversion from the original 1053 nm light to the third harmonic light (351 nm). Therefore, a tri-wavelength broadband AR coating that works simultaneously at the target wavelengths (1053 nm, 527 nm and 351 nm) is extremely necessary.^{9,10} In this AR coating preparation, besides considering the refractive index of coatings, other strictly restricted conditions must be regarded,¹¹ for instance, the coating materials must have zero absorption in ultraviolet – visible – near infrared region, high laser induced damage threshold, and simple deposition process as possible to ensure the accurate control of film thickness. Therefore not only the suitable coating materials are extremely limited in this field, but also the methods of regulation on refractive index tend to simple sol-gel process. Other methods such as ion etching and LBL assembly have been rarely reported because of the

obvious difficulty in preparing high-quality coatings with large aperture.

SiO₂ is the most widely studied AR coating material in the high power laser system. Its regulation on refractive index mainly focused on the Thomas's sol-gel method from which the refractive index can be adjusted from 1.22 to 1.44 by mixing based-catalyzed SiO₂ colloid particles and acid-catalyzed SiO₂ linear polymer.¹² Recently, Jiang's group¹³ successfully obtained a double-wavelength broadband SiO₂ AR coating system with transmittance of 99.6% and 99.8% at 527 nm and 1053 nm respectively by adopting Thomas's method. But, this method involved the ammonia removal by refluxing the sol so that it was not easy for large-scale sol preparation.

Another interesting AR coating material in the high power laser system is MgF₂, whose main advantage over SiO₂ is the better transmission and perfect laser damage resistance in the UV region.^{14,15} But, its normal regulation method of the refractive index relied on the nanoscale decomposition of MgF₂ precursor in film in a heat treatment process,^{16,17} which was unfavourable for the fabrication of the tri-wavelength broadband AR coating owing to the difficulty in accurately controlling the thickness of each layer. Through further research and analysis of the related work in recent years, we found that the heat treatment to the MgF₂ sols always accompanied with the tendency of network structure formation,¹⁸⁻²² which provided a new possibility to realize the regulation of refractive index. However, this approach was curiously overlooked before, which may be presumably related to the difficulty in handling the delivery process to obtain high-quality MgF₂ sol.

In this work, the refractive index of MgF_2 coatings was tuned from 1.38 to 1.2 through the heat treatment of MgF_2 sol. Compared with the Tsuyoshi Murata' work²² that lowered the refractive index of MgF_2 coating through formation of bigger spherical particles by autoclaving, the biggest difference in our work was the intervention of carboxyl groups, which existed in the high-concentrations reaction system and could guide the MgF_2 nanocrystals assemble to hollow vesicles structures. It is worthy of mentioning that this high-concentrations reaction system is necessary for the tri-wavelength broadband AR coating system owing to the requirement of thick layer, but its delivery process is very challenging since the big clusters are easily formed and will seriously affect the optical performance. Furthermore, using two MgF_2 layers with refractive index of 1.34 and 1.2 as bottom and top layer respectively, a double-layer tri-wavelength broadband AR coating on quartz substrate had been realized, and meanwhile the transmittance at 351 nm, 527 nm and 1053 nm could achieve 99.54%, 98.65%, and 98.58% respectively.

Experimental section

Materials: Magnesium acetate, methanol and hydrofluoric acid were purchased from Alfa-Aesar, and were used as received without further purification.

Preparation of MgF_2 sol: the high-concentration MgF_2 sol (0.38 M) was firstly prepared at room temperature: 8.96g $\text{Mg}(\text{CH}_3\text{COO})_2$ was first dissolved in 120 mL distilled methanol, then added aqueous 4.8 g HF to form MgF_2 sol under vigorous stirring. Then the obtained MgF_2 sol was transferred into a Teflon-lined stainless steel autoclave and maintained at 150°C for required time to regulate the refractive index. After being cooled down to room temperature naturally, the sol was left in a closed plastic container and aged at 5°C for two weeks for coating preparation.

Coating preparation: quartz substrates were cleaned by ethanol in ultrasonic cleaner for 10 min and wiped carefully before dip-coating. Then sols were coated on the well-cleaned quartz substrates by dip coating at a desired withdraw rate. To prepare double-layer tri-wavelength AR coating, the heat treatment time to sols for top and bottom layers were selected as 5 h and 24 h respectively.

Characterization: Powder X-ray diffraction (XRD) (Bruker D8 Advance), transmission electron microscopy (TEM and HRTEM, JEOL-2100F, 200 kV), and dynamic light scattering (DLS Malvern Instruments) were used to characterize sol. UV-Vis spectrometer (U4100, Hitachi), atomic-force microscopy (XE-100, PSIA) and spectroscopic ellipsometer (SE 850, Sentech) were used to measure the transmission spectra, surface morphology and reflective index of the AR coating.

Results and Discussion

3.1 Structure evolution of Sol Particles

To understand the regulation mechanism of refractive index of MgF_2 coatings, the particle structure evolution in sol must be determined at first. At room temperature, the reaction of $\text{Mg}(\text{CH}_3\text{COO})_2$ with HF directly resulted the formation of MgF_2 nanocrystals of size 1~3 nm as shown in Fig. 1(a). The lattice fringes spacing 0.326 nm of the selected area shown in Fig. 1(e) can be well indexed to (110) plan of the tetragonal structure of MgF_2 . During the heat treatment at 150°C for 5 h to the sol, nanocrystals began to assemble along a ring as Fig. 1(b) displayed, some of which interconnected closely to gather into hollow vesicles, even though the vesicles were not too much and not very complete. Prolonging the heat treatment time to 15 h, hollow vesicles structure shown in Fig. 1(c) had become the predominant structure. When the heat treatment time lasts to 24 h (Fig. 1(d)), the assembly process of hollow vesicles structure almost finished, meanwhile the lattice spacing of 0.326 nm of (110) planes in the Fig. 1(f) revealed that the MgF_2 phase was unchanged in the assemble process.

To further confirm the non-existence of other possible reaction in the heat treatment process, these MgF_2 gel powders were further characterized by XRD, shown in Fig. 2. The gel powder at room temperature showed broad diffraction peaks at the expected 2θ of 27.3°, 40.4°, 53.5°, 60.6° and 68.1°, which can respectively indexed to (110), (111), (211), (002) and (301) facets of crystalline magnesium fluoride (PDF: 41-1443),²² no other products were detected. Prolonging the reaction time of the heat treatment to the sol at 150°C, beside the above

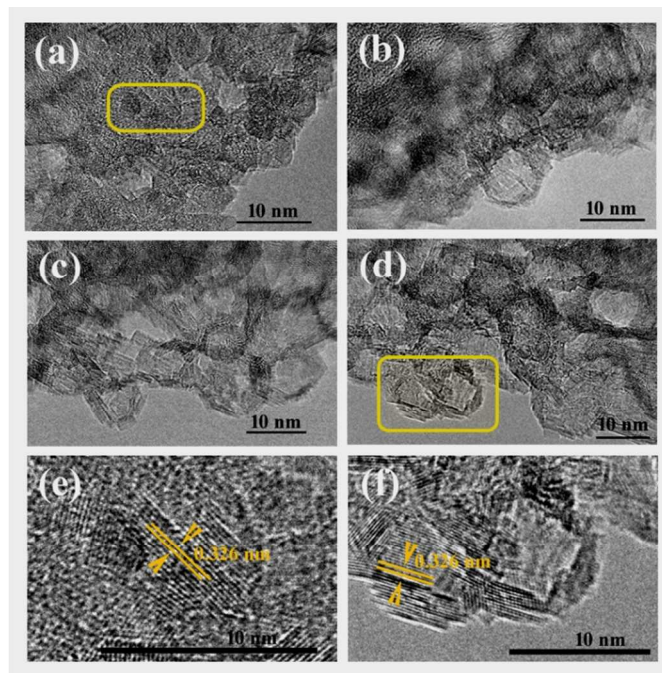


Fig. 1 TEM images of the structure evolution of 0.38 M MgF_2 sols with different heat treatment time: (a) at room temperature; (b) 150°C for 5 h; (c) 150°C for 15 h and (d) 150°C for 24 h. (e) HRTEM image of the selected in Fig. 1(a). (f) HRTEM image of the selected shown in Fig. 1(d).

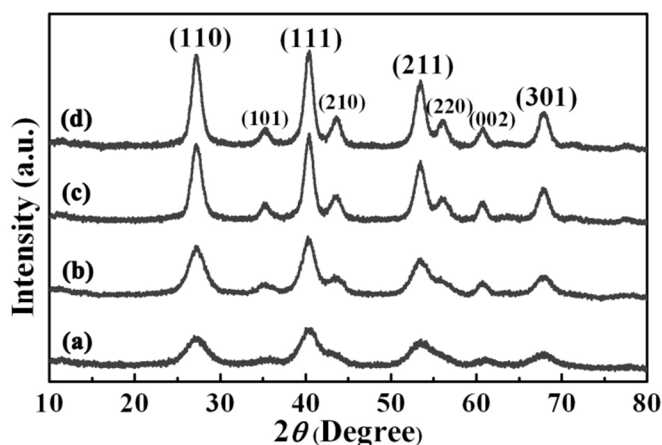


Fig. 2 XRD patterns of the structure evolution of 0.38 M MgF_2 gel powders as-prepared with different heat treatment time: (a) at room temperature; (b) 150°C for 5 h; (c) 150°C for 15 h and (d) 150°C for 24 h.

diffraction intensity became more pronounced and three other reflections (101), (210) and (220) appeared more distinctly, still no other products were detected, meaning that the heat treatment process could not involve any disadvantageous reactions.

To monitor the real self-assemble behavior of the hollow vesicles structure, DLS technique that can *in-situ* provide the size distributions of the intermediates in the sol was further applied (Fig. 3). After reaction at room temperature, the hydrodynamic diameters of the sol possessed a single distribution with the peak value of 2 nm, revealing that the nanocrystals as the primary particles were well dispersed in the sol at this stage. After reaction for 5 h at 150°C, the hydrodynamic diameter of the sol particles presented a bimodal size distribution, implying the existence of two distinct diffusing species in the sol. The primary distribution in the

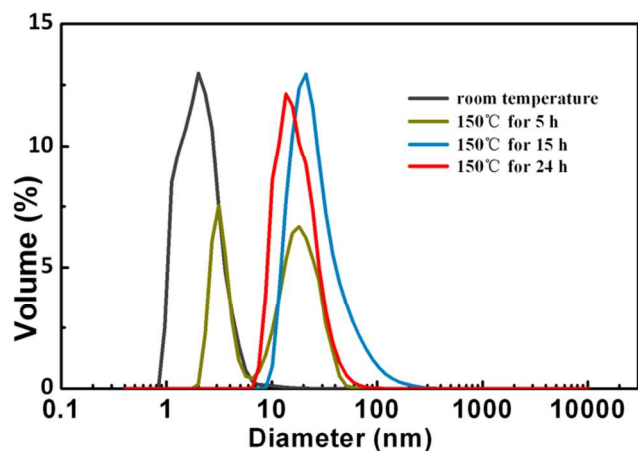


Fig. 3 Evolution process of particles hydrodynamic diameter of 0.38 M MgF_2 sols as-prepared with different heat treatment time.

small size range should result from the MgF_2 nanocrystals that were assembling. Another distribution with the peak value of about 18 nm should be the appearance of some hollow vesicles. In the case of reaction for 15 h at 150 °C, there was only a single distribution with a peak value of 21 nm in the large size range, indicating that almost all the primary particles self-assembled into the larger hollow vesicles at this stage. When the reaction lasted to 24 h, the hollow vesicles became more regular and compacted, leading to slightly decreased peak size. Such a time-dependent size distribution evolution agreed well with the TEM observations shown in Fig. 1. As a result, it can be concluded that the heat treatment process played a key role in the formation of hollow vesicle structure. Generally, in this heat treatment process, Ostwald ripening²³ mechanism should be the most predictable process as reported by the Tsuyoshi Murata' work,²² but why self-assemble process could occur here ?

To explain this self-assembly process, concentrations-dependent heat treatment was further investigated by TEM observations, as shown in Fig. 4. In 150°C heat treatment process, with the reactant concentration increasing, the self-assemble process became more obvious (except the 0.42 M gel), while Ostwald ripening process as the possible energy released way was inhibited more seriously. Considering the acetic acid molecules generated in the room temperature reaction, a possible explanation based on the adsorption of acetate ions was proposed here. The carboxyl groups adsorbed by the magnesium sites on the nanocrystal surfaces can inhibit these adsorption sites as active centers for further growth,²⁴ as description in Scheme 1. When the reactant concentration was low, only a small amount of acetate ions adsorbed on the nanocrystals surfaces, resulting in a weak inhibiting effect on nanocrystal growth. With the reactant concentration increasing, ions adsorption also increased. For lots of existence of adsorbed acetate ions, shielding effect between the nanocrystals surfaces cannot be ignored,²⁵ leading to only edge-to-edge interconnection like a soccer that finally self-assembled into the

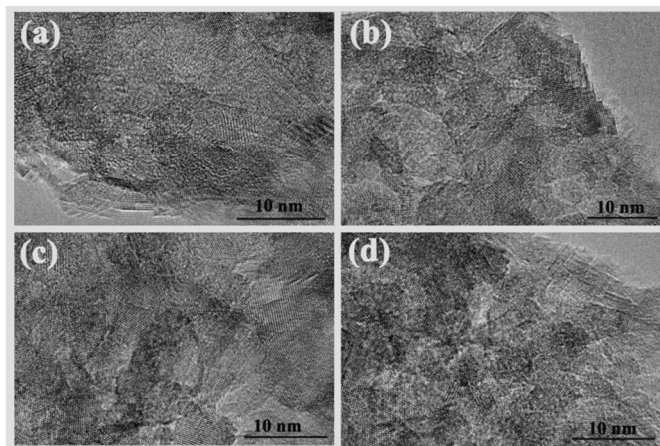
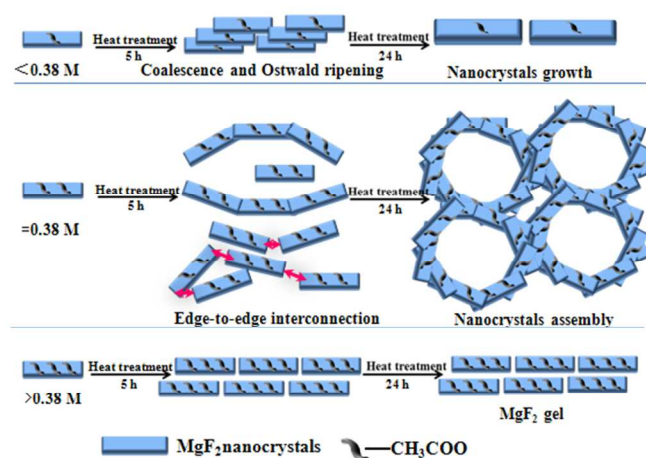


Fig. 4 TEM images of the structure evolution of MgF_2 sols with different concentrations: ((a)-(c)) 0.18 M; 0.3 M and 0.38 M MgF_2 sols obtained at 150°C for 24 h. (d) 0.42 M MgF_2 gel obtained at 150°C for 24 h.



Scheme 1 Evolution mechanism of colloidal MgF_2 nanocrystals in heat treatment process.

hollow vesicles structure. With the reaction concentration further increasing, ions adsorption became more serious, shielding effect would expand to the whole nanocrystals, which made the Ostwald ripening and self-assemble process completely disappear. At this stage, to reduce the free energy of the system, MgF_2 gel forms.

3.2 Refractive index regulation of MgF_2 single film

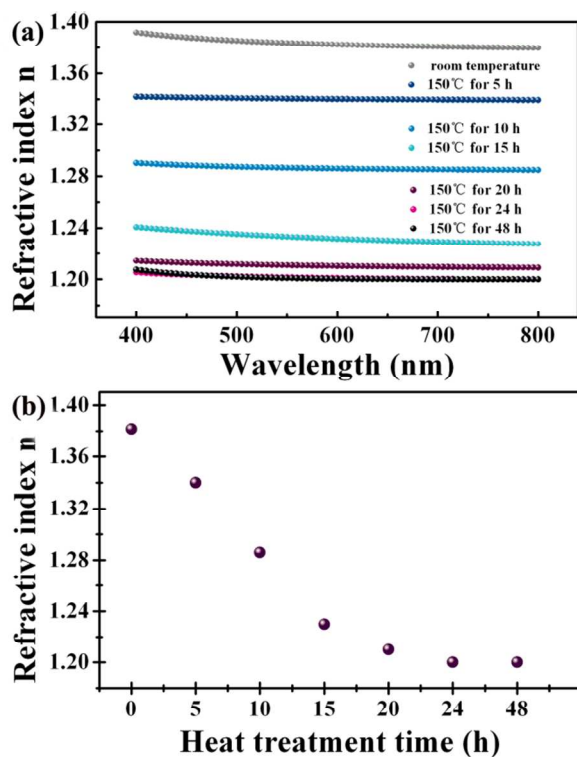
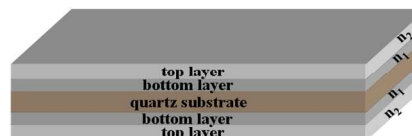


Fig. 5 Effect of heat treatment time on refractive index of AR coatings (derived from 0.38 M MgF_2 sols): (a) dispersion curves over 400 nm to 800 nm; (b) refractive index at 633 nm.

Spectroscopic ellipsometry was used to measure the refractive index of MgF_2 coatings derived from 0.38 M sols with different heat treatment time at 150°C . It can be seen that in Fig. 5, with the treatment time prolonging, the effective refractive index of the MgF_2 coating decreased rapidly, then slowed down and approached a stable. Especially at 633 nm, it decreased from initial 1.38 to minimum 1.2. Through analysis in the self-assembly process of nanocrystals in sol and the coating drying process in dip coating, the refractive index regulation mechanism of MgF_2 coatings can be summarized as follows. The sol prepared at room temperature was comprised of many small nanocrystals that preferred to form packed coating nearly without pores, thus the refractive index of the coatings could be 1.38 high as the bulky material. In the heat treatment process, with the hollow vesicles increasing in sol, more and more nanoporous structures were created in the AR coatings, and then reduced the refractive index gradually. Although the hollow vesicles structures have been formed completely at the reaction of 15 h, the refractive index reached the minimum at the reaction of 24 h. This is because that the hollow structure formed at 24 h could be more compacted, and easier to be preserved in the drying process.

3.3 Tri-wavelength AR coating



Scheme 2 Schematic diagram of tri-wavelength AR coating.

In order to achieve the simultaneous antireflection at three wavelengths, a double-layer system is the simplest and feasible design, as shown in Scheme 2. With the aid of film design software Filmstar, the corresponding refractive index and thickness of the two layers have been designed, as shown in Table 1.

Table 1 Refractive index, thickness and transmittance of double-layer tri-wavelength AR coatings modeled by Filmstar.

Bottom layer		Top layer		$T_{351\text{ nm}}$	$T_{527\text{ nm}}$	$T_{1053\text{ nm}}$
n_1	Thickness (nm)	n_2	Thickness (nm)			
1.35	93.07	1.26	223.52	98.96	97.66	98.12
1.34	96.76	1.26	220.22	98.91	97.89	97.97
1.33	99.15	1.26	219.08	98.88	98.15	97.77
1.32	101.66	1.26	217.94	98.89	98.35	97.53
1.35	81.37	1.20	253.3	99.19	97.93	98.99
1.34	95.69	1.20	231.9	99.84	98.69	99.01
1.33	100.34	1.20	229.2	99.81	98.29	98.09
1.32	104.75	1.20	227.4	99.78	98.47	98.74
1.35	82.92	1.15	264.46	99.43	98.23	98.94
1.34	84.23	1.15	262.91	99.57	98.45	98.91
1.33	86.90	1.15	258.41	99.84	98.58	98.98
1.32	89.46	1.15	252.72	99.98	98.68	99.01

Considering the refractive index range obtained in Fig. 5, bottom and top layers with refractive index of 1.34 and 1.20 and thickness of 95.69 nm and 231.9 nm was the best choice to achieve the transmittance of 99.84%, 98.69% and 99.01% at 351 nm, 527 nm and 1053 nm respectively. According to this design requirement, 0.38 M MgF_2 sol treated at 150°C for 5 h and 0.38 M sol treated at 150°C for 24 h have been chosen for

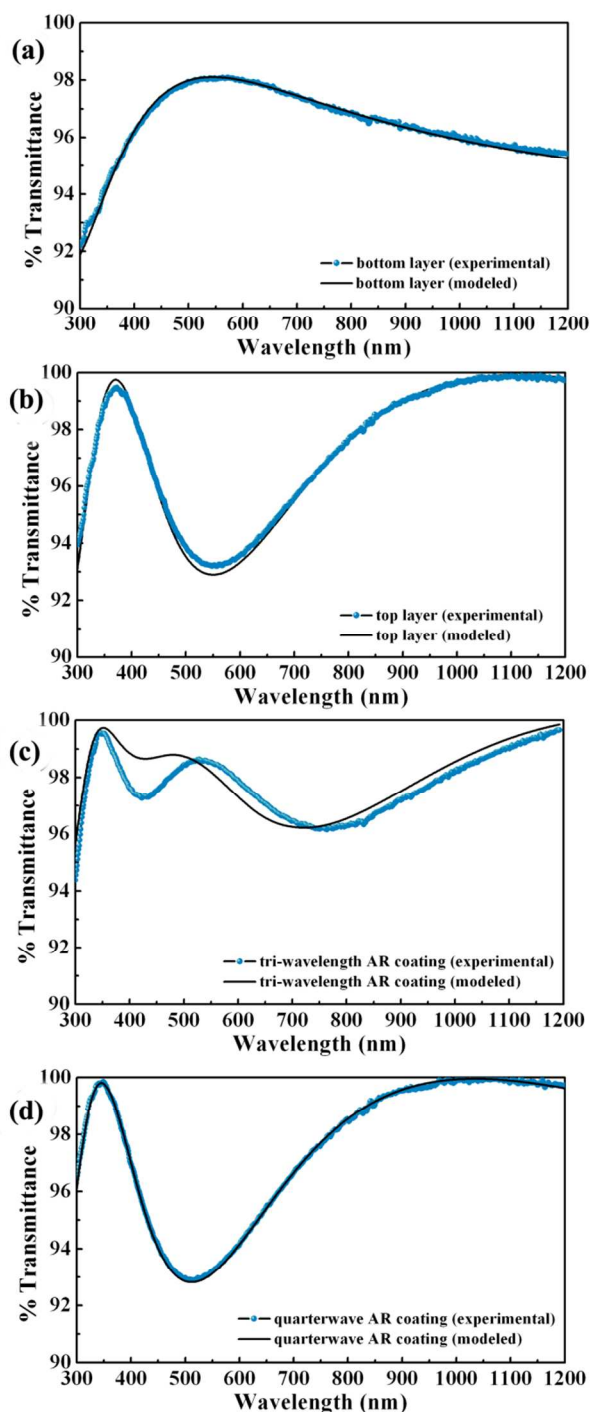


Fig. 6 Transmittance spectra of the AR coatings: (a) single bottom layer; (b) single top layer; (c) double-layer and (d) single quarterwave layer.

the bottom and top layers. Then the optimal dip-coating speeds were obtained to adjust the thickness of bottom and top layers with a central wavelength of 513 nm and 1113 nm as designed. After this, the double layer AR coating can be realized by sequentially coating the bottom and top layers onto a quartz substrate. The relevant results are presented in Fig. 6 and Fig. 7. For single bottom and top layers on quartz substrates, the experimental transmittance spectra with peak values of 98.03% and 99.8% are both in good agreement with that of the designs at $n=1.34$ and $n=1.2$, as shown in Fig. 6(a) and Fig. 6(b). In addition, directly related to the optical quality, the surface roughness was tested with AFM. As displayed in Fig. 7(a) and Fig. 7(b), there are many particle-like bumps on both surfaces, wherein the root-mean-square roughness R_q of bottom layer is about 1.2 nm, smoother than the top layer with R_q about 2.36 nm. This difference of two layers can be ascribed to the self-assembly degree in sols: the larger the MgF_2 assembly structure is, the rougher the coatings would be. In general, both of the coatings are uniform and smooth enough to be used for preparing double-layer coating.

For the prepared double-layer AR coating, the transmittance achieved 99.54%, 98.65% and 98.58% at 351 nm, 527 nm and 1053 nm, as displayed in Fig. 6(c), which was slightly lower than the designed sample. It is well known that even small deviation from the optical design would lead to big transmittance deviation of multilayer AR coatings. In practical fabrication, the thickness error in one or both of the layer and dispersion relation without considering in the designed sample both existed unavoidably. So this small deviation in our work was acceptable. In addition, compared with the single bottom and top layers, the R_q value of this double-layer coating was increased to 3.34 nm owing to the cumulative effect, but still good enough to meet the requirements.²⁶

As a reference, a single-layer quarterwave AR coating with a central wavelength of 1053 nm was fabricated on quartz

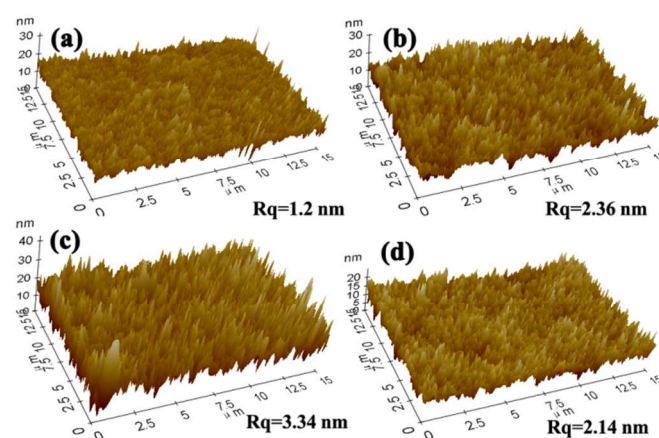


Fig. 7 AFM images of the AR coatings: (a) single bottom layer; (b) single top layer; (c) double-layer and (d) single quarterwave layer.

substrate using 0.38 M sol treated at 150°C for 15 h, the refractive index of which is 1.23, satisfying the principle: $n_c = (n_a n_s)^{0.5}$, where n_c , n_a , and n_s are the refractive index of the coating, air, and substrate, respectively. As shown in Fig. 6(d) and Fig. 7(d), this traditional quarterwave AR coating possessed excellent transmittance at 1053 nm and 351 nm and low R_q about 2.14 nm. But, its transmittance at 527 nm was too low to meet the practical need. By contrast, the advantage of the double-layer broadband AR coating is immediately apparent.

Conclusions

In this work, we showed that MgF_2 hollow vesicle structures generated by heat treating the high-concentrations MgF_2 sol could be employed to fabricate nanoporous coatings with tunable refractive index over the range 1.38 to 1.2. We also demonstrated that when the refractive index of the bottom and top layers were chosen to 1.34 and 1.2, the transmittance of this double-layer tri-wavelength AR coating achieved 99.54%, 98.65% and 98.58% at 351 nm, 527 nm and 1053 nm, respectively, making it suitable for use in the high power laser system. What we need to point out is that the realization of this double-layer tri-wavelength AR coating completely relies on the effective heat treatment process, which is particularly amenable to the creation of large-area uniform coatings with precise control of thickness.

Notes and references

^a Key Laboratory of Carbon Materials, Institute of Coal Chemistry, Chinese Academy of Sciences, Taiyuan 030001, China

^b University of Chinese Academy of Sciences, Beijing 100049, China

* Corresponding author. E-mail: xuyao@sxicc.ac.cn

1. S. Guldin, P. Kohn, M. Stefik, J. Song, G. Divitini, F. Ecarla, C. Ducati, U. Wiesner and U. Steiner, *Nano letters*, 2013, **13**, 5329-5335.
2. H. Hattori, *Advanced Materials*, 2001, **13**, 51-54.
3. J. Hiller, J. D. Mendelsohn and M. F. Rubner, *Nature materials*, 2002, **1**, 59-63.
4. C. Sanchez, C. Boissière, D. Grosso, C. Laberty and L. Nicole, *Chemistry of Materials*, 2008, **20**, 682-737.
5. S. Kitamura, Y. Kanno, M. Watanabe, M. Takahashi, K. Kuroda and H. Miyata, *ACS Photonics*, 2014, **1**, 47-52.
6. H. Y. Hsueh, H. Y. Chen, M. S. She, C. K. Chen, R. M. Ho, S. Gwo, H. Hasegawa and E. L. Thomas, *Nano letters*, 2010, **10**, 4994-5000.
7. S. Walheim, *Science*, 1999, **283**, 520-522.
8. Y. Du, L. E. Luna, W. S. Tan, M. F. Rubner and R. E. Cohen, *ACS nano*, 2010, **4**, 4308-4316.
9. I. M. Thomas, *The International Society for Optical Engineering*, 1997, **3136**, 215-219.
10. P. Belleville, P. Prene, C. Bonnin and Y. Montouillout, *Materials Research Society*, 2002, **726**, 369-380.
11. H. G. Floch, P. F. Belleville, J. J. Priotton, P. M. Pegon, C. S. Dijonneau and J. Guerain, *American Ceramic Society Bulletin*, 1995, **74**, 84-89.
12. I. M. Thomas, *Applied optics*, 1992, **31**, 6145-6149.

13. X. X. Zhang, S. Cai, D. You, L.-H. Yan, H. B. Lv, X. D. Yuan and B. Jiang, *Advanced Functional Materials*, 2013, **23**, 4361-4365.
14. M. J. Dodge, *Applied optics*, 1984, **23**, 1980-1985.
15. N. Kaiser, *The International Society for Optical Engineering*, 1994, 2253, 722-730.
16. J. D. Bass, C. d. Boissiere, L. Nicole, D. Grosso and C. m. Sanchez, *Chemistry of Materials*, 2008, **20**, 5550-5556.
17. S. Fujihara, M. Tada and T. Kimura, *Thin Solid Films*, 1997, **304**, 252-255.
18. D. Grosso, C. Boissiere and C. Sanchez, *Nature materials*, 2007, **6**, 572-575.
19. J. Noack, K. Scheurell, E. Kemnitz, P. Garcia-Juan, H. Rau, M. Lacroix, J. Eicher, B. Lintner, T. Sontheimer, T. Hofmann, J. Hegmann, R. Jahn and P. Löbmann, *Journal of Materials Chemistry*, 2012, **22**, 18535.
20. H. K. Raut, S. S. Dinachali, K. K. Ansah-Antwi, V. A. Ganesh and S. Ramakrishna, *Nanotechnology*, 2013, **24**, 505201.
21. J. Noack, F. Emmerling, H. Kirmse and E. Kemnitz, *Journal of Materials Chemistry*, 2011, **21**, 15015.
22. T. Murata, H. Ishizawa, I. Motoyama and A. Tanaka, *Journal of Sol-Gel Science and Technology*, 2004, **32**, 161-165.
23. M. Kahlweit, *Adv. Colloid Interface Sci.*, 1975, **5**, 1-35.
24. I. Sevonkaev and E. Matijevic, *Langmuir : the ACS journal of surfaces and colloids*, 2009, **25**, 10534-10539.
25. E. Kemnitz, S. Wuttke and S. M. Coman, *European Journal of Inorganic Chemistry*, 2011, **2011**, 4773-4794.
26. B. Xiao, B. Xia, H. Lv, X. Zhang and B. Jiang, *Journal of Sol-Gel Science and Technology*, 2012, **64**, 276-281.